FULL PAPER

Conductivity of SU-8 Thin Films through Atomic Force Microscopy Nano-Patterning

*Cristina Martin-Olmos, L. Guillermo Villanueva, Peter D. van der Wal, Andreu Llobera, Nico F. de Rooij, Jürgen Brugger, and Francesc Perez-Murano**

Processing flexibility and good mechanical properties are the two major reasons for SU-8 extensive applicability in the micro-fabrication of devices. In order to expand its usability down to the nanoscale, conductivity of ultra-thin SU-8 layers as well as its patterning by AFM are explored. By performing local electrical measurements outstanding insulating properties and a dielectric strength 100 times larger than that of SiO_2 are shown. It is also demonstrated that the resist can be nano-patterned using AFM, obtaining minimum dimensions below 40nm and that it can be combined with parallel lithographic methods like UV-lithography. The concurrence of excellent insulating properties and nanometer-scale patternability enables a valuable new approach for the fabrication of nanodevices. As a proof of principle, nano-electrode arrays for electrochemical measurements which show radial diffusion and no overlap between different diffusion layers are fabricated. This indicates the potential of the developed technique for the nanofabrication of devices.

1. Introduction

Polymers are key materials in micro- and nano-fabrication of electronic and mechanical devices. Polymer-based resists are primarily used to transfer patterns to substrates via lithography and subsequent etching, deposition or implantation.[1,2] However, polymers can also be used as structural layer(s) of mechanical micro-devices.[3–5] The majority of the techniques employed to shape the polymer layers are based on the exposure of the resist to an energetic radiation, as photons in optical lithography (OL) or to a beam of electrons in electron beam lithography (EBL). Upon exposure, the resist endures fundamental changes in its structure, like scission of the chains (positive resists) or cross linking (negative resists), which allows the removal of the exposed (positive) or non-exposed (negative) part of the resist via chemical dissolution during development. Patterning such polymers with deep sub-micrometric resolution is a necessary condition for many applications, including CMOS fabrication, and has become a major struggle for most research groups, due to the high cost-of-ownership of the specialized equipment that allows such resolution (e-beam or deep UV). As a result, in recent years we have witnessed the development of different novel lithographic methods that provide good resolution with low operational and ownership costs as for example nanoimprint lithography,[6,7] nanostencil lithography[8,9] or scanning probe lithography (SPL).[10,11]

Almost since its invention, atomic force microscopy (AFM) has attracted a lot of attention as a potential nanolithography tool due not only to the very small features achievable (below 10 nm[12]) but also to the possibility to perform morphological and physical characterization of the as-formed patterns by the same tip that performs the lithography. Different types of SPL have been demonstrated, like local oxidation[13] or reduction,[14] dip-pen nanolithography,[15] nano-scratching,[16] thermomechanical deformation,[17,18] deposition[19] or desorption,[12] or local chemical lithography.[20] All of them, though very precise, suffer from a very low throughput (they are serial processes) that limits their applicability. In order to improve SPL techniques' throughput, it is possible to utilize probe arrays[21,22] or to combine them with other faster techniques like EBL or OL.

Poly-(methyl methacrylate) (PMMA) is a good option for the combination of SPL and EBL. In a previous work,[23] we have presented an study of the mechanism of local modification of PMMA by AFM under the application of a voltage between tip and substrate. It was shown that the polymer can be locally dissolved when applying a high enough voltage. By analyzing the current flowing between tip and substrate it was concluded that the modification is caused by an electrochemical reaction, provided that a water meniscus between tip and surface is formed. The water meniscus in combination with the high electrical field created by the application of voltage "supplies" a high density of ionic species. These ionic species (mainly OH- ions) are transported through the PMMA and cause the oxidation of the underlying silicon. When the applied voltage is high enough, an additional electrochemical reaction occurs that causes the dissolution

Dr. C. Martin-Olmos, Dr. A. Llobera, Prof. F. Perez-Murano
Institut de Microelectrònica de Barcelona (CNM-IMB-CSIC)
Campus de la Universitat Autònoma de Barcelona
E-08193 Bellaterra, Spain
E-mail: Francesc.Perez@csic.es
Dr. C. Martin-Olmos, Dr. L. G. Villanueva, Prof. J. Brugger
Laboratory of Microsystems
École Polytechnique Fédérale de Lausanne (EPFL)
CH-1015 Lausanne, Switzerland
Dr. P. D. van der Wal, Prof. N. F. de Rooij
Sensors, Actuators and Microsystems Laboratory
École Polytechnique Fédérale de Lausanne (EPFL)
CH-2002 Neuchâtel, Switzerland

DOI: 10.1002/adfm.201102789

of PMMA. Other works have shown that PMMA can also be modified using AFM due to thermal effect[24,25] or indentation.[26]

In this paper, we study the nanopatterning of SU-8 thin films by AFM. SU-8 is an epoxy-based negative resist widely used for MEMS fabrication[27] because of its high aspect ratio,[28] good mechanical properties[29] and etching resistance.[30] It can be patterned via OL and EBL[31] but, to our knowledge, SPL has only been used on SU-8 to create superficial patterns of less than 4 nm in depth, which has limited practical applications in, for example, data storage.[32]

As it is demonstrated below, ultra-thin layers of SU-8 are an outstanding material to be used in the fabrication of nanodevices. We show that they have very good insulating properties and extremely high dielectric strength, and that they can be patterned with AFM. We also show the existence of two mechanisms governing such patterning, i.e., mechanical material displacement and electrochemical dissolution. Finally, we also show a proof of concept of the possibilities that using these ultra-thin layers entails, by fabricating nanoelectrode arrays with a purely polymeric insulating structure.

2. Results

2.1. Insulating Properties of SU-8 Thin Films

In order to investigate the lithographic possibilities of the resist using AFM, we first study the insulating properties of these very thin layers of SU-8. In order to do so, samples with well-defined nanoelectrodes (see Experimental Section and Supporting Information) are fabricated (**Figure 1**a). We then contact one electrode with a conductive AFM tip, and apply a voltage ramp while monitoring the current flowing through the tip with a low noise amplifier. The area of the electrodes (around 450 nm in diameter) is optimal to allow easy contact with the AFM probe and to obtain a proper level of current. A much larger electrode size (several micrometers squared) would cause the electronic conductance to be dominated by possible point-defects on the film resist.

Figure 1b and c. show typical *I–V* curves performed on top of exposed and non-exposed 20 nm thick SU-8 films. The first part of the *I–V* curves is dominated by the input noise of the transconductance amplifier used in the experiments. For higher applied voltages, a Fowler–Nordheim conduction law is observed. By closely analyzing that region (Figure 1c and Supporting Information), it is possible to extract a dielectric energy barrier that, for the exposed resist, is two times that of the non-exposed. Finally, in the case of the non-exposed resist, dielectric breakdown is observed for V ≳ 35 V; whereas no breakdown is observed for the exposed resist.

2.2. Indentation Experiments

The second set of experiments consists on performing series of force vs. distance curves with the AFM on the surface of the SU-8 resist. While performing the curves, DC voltage is applied between the tip and the substrate (ranging from 0V up to 45V, substrate positive) and simultaneously, the electrical current flowing through the tip is registered. This is done for the four different types of samples (non-exposed SU-8 on Si, exposed SU-8 on Si, non–exposed SU-8 on Au coated Si and exposed SU-8 on Au coated Si, see Experimental Section), although in the manuscript we only present and analyze the results obtained for SU-8 deposited on gold-coated silicon substrates. The rest of results are included in the Supporting Information.

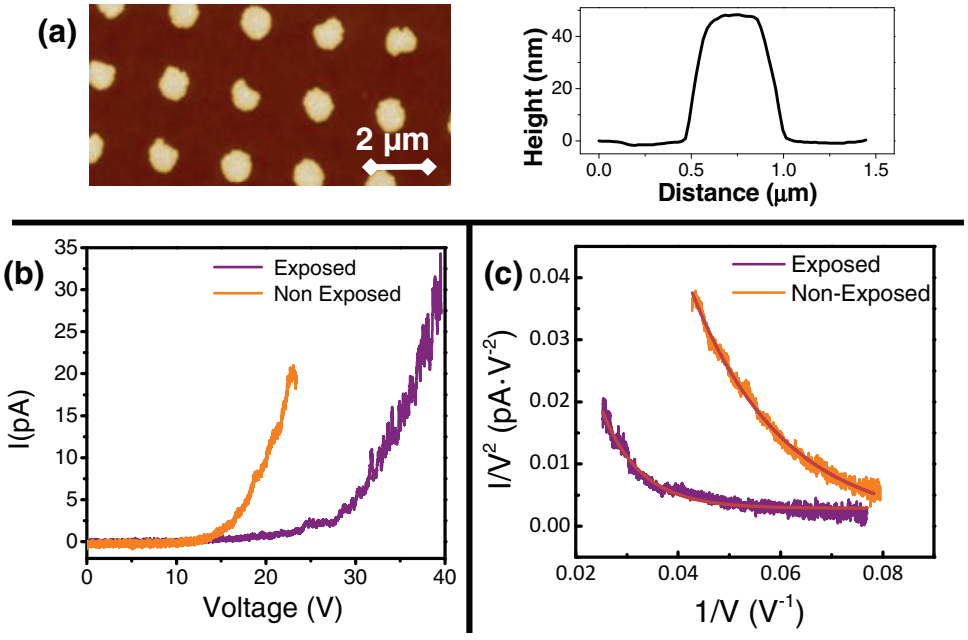

Figure 1. Study of SU-8 conductivity: a) AFM topography image of the metallic electrodes deposited by nanostencil lithography on top of a very thin SU-8 layer. Their typical size is 450 nm diameter and 40 nm thick as shown in the cross section graph. b) *I–V* curves on 20 nm thick layers of exposed and non exposed photoresist (purple and orange respectively). c) Fit of the experimentally obtained current versus voltage data to a Fowler-Nordheim tunneling law for non-exposed (orange) and exposed (purple) 20 nm thick SU-8 layer.

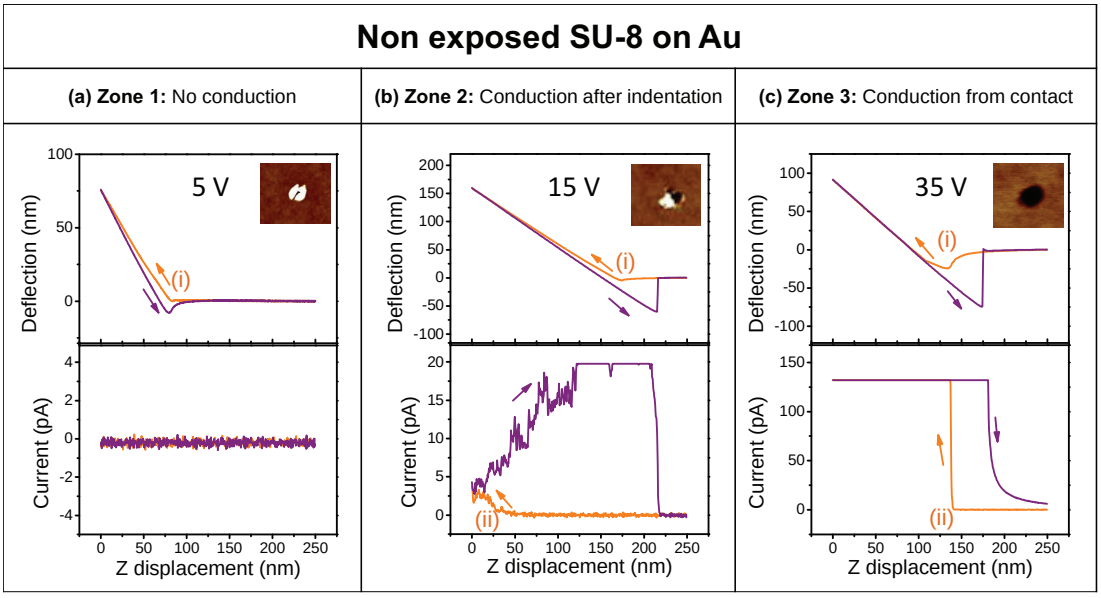

Figure 2. Non-exposed resist behavior: Exemplary cases of the three different behavioral regions for non-exposed SU-8 on gold-coated silicon substrates (non-anodizable substrates). a) No conduction. No measurable current can be detected beyond the transconductance amplifier input noise limit. Protrusion can be observed around the indented hole due to mechanical displacement of the resist. The bias voltage applied in this particular case is 5 V. b) Conduction after indentation. Electrical current is not detected simultaneously to the tip physically contacting the resist. Once conduction starts, current grows continuously until loss of physical contact, due to electrical dissolution of the resist, which effectively increases contact area. Also for this reason, protrusions are reduced. Bias voltage applied is 15 V. c) Conduction from contact. For high-enough voltages, conduction starts simultaneously to physical contact of the tip with the resist. This is due to dielectric breakdown combined with electrochemical dissolution of the resist. Saturation of the measured current occurs, together with total removal of the protrusions. Bias voltage applied is 35 V.

2.2.1. Non-Exposed SU-8

When the applied voltage is small, no significant conduction is observed, as it can be seen in **Figure 2**a. After a certain threshold voltage (which is different from sample to sample but typically between 10 and 15 V), conduction can be observed if, and only if, a sufficient long indentation is performed in the resist. Figure 2b illustrates this behavior: no measurable current is observed while the tip is indenting the resist (between point (i) and (ii)). Conduction can be measured approximately at the same time that the tip enters in contact with the substrate (when the slope of the deflection curve is equal to one). It is observed that the distance between points (i) and (ii) decreases with voltage and for sufficiently high voltages (typically above 35 V), conduction and tip deflection are observed to start simultaneously, as it is shown in Figure 2c.

These three different behaviors described are directly correlated with the resulting pattern in the non-exposed resist, as can be observed in the insets of Figure 2. Depending on the voltage we can indent (low voltages), partially remove the resist (medium voltages) or fully remove the resist (high voltage). For low voltages (Figure 2a) there is no current measured while the force curve is showing an indentation and the resulting pattern is an indented dot. For medium voltages (Figure 2.b) current starts to flow after a certain part of the resist is indented and some of it is dissolved. For high voltages (Figure 2c) current starts almost simultaneously with the tip contacting the resist and it is removed completely.

2.2.2. Exposed SU-8

When performing the indentation experiments on exposed SU-8, the behavior of the resist shows some similarities with the non-exposed case, but also some differences. For small voltages, as in the previously described case, there is no measurable current flowing through the tip. There is also in this case a threshold voltage beyond which conduction is detected. The value of the threshold voltage is, although different from sample to sample, larger than in the previous case (typically between 15 and 25 V). The "delay" between physical contact and electrical contact described previously can also be observed for both types of substrates (distance between points (i) and (ii) in **Figure 3**). However, this "delay" is now independent of the value of applied voltage. Finally, the third region described before, in which conduction and deflection start simultaneously, cannot be observed for the exposed resist.

Figure 3 shows an exemplary case of force vs. distance curve. The current grows steeply to reach an approximately constant value that is kept until contact is lost. This is in contrast to what can be seen in Figure 2b for non-exposed resist, where the current grows until contact is lost.

2.3. AFM Nanopatterning of Thin SU-8 Films

In order to explore the possibilities that this resist offers to perform AFM based lithography, single dots are patterned. **Figure 4** shows AFM topography images of some typical results of the patterning of dots on non-exposed (Figure 4a) and exposed SU-8 (Figure 4b). The dots are fabricated by making indentations at each position while applying a constant voltage between tip and substrate. All the points in the same horizontal line are obtained with the same voltage. Figure 4a shows the difference

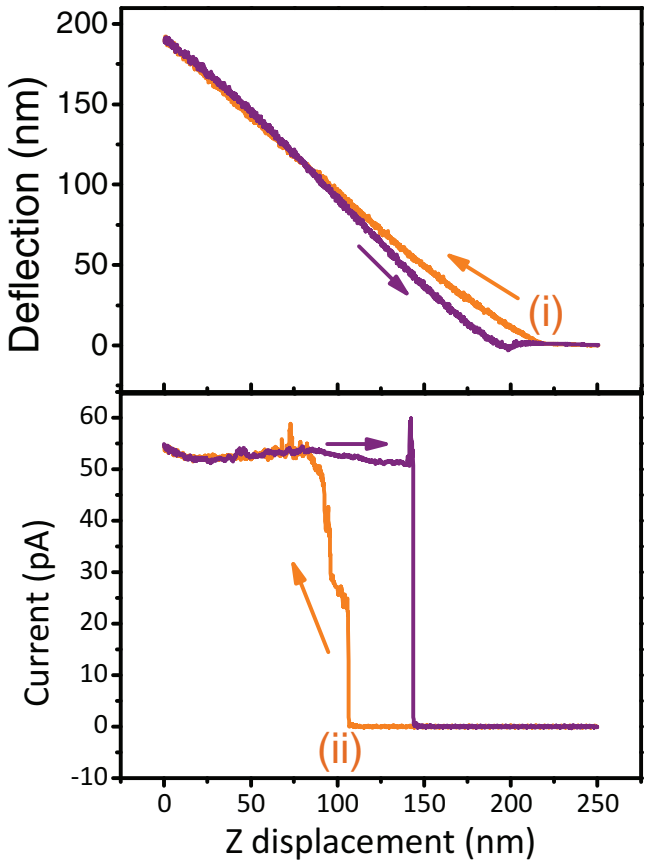

Figure 3. Exposed resist behavior: Force/Current vs. distance curve taken on samples with exposed SU-8 on gold-coated silicon substrate. The applied voltage (40 V) is higher than the threshold for conduction. As for non-exposed resist (Figure 2), the current starts flowing (ii) after the tip enters in contact with the resist (i). The current grows steeply initially until it saturates at a value that is kept until electrical contact is abruptly lost.

between the three regions described in the previous section (see also Supporting Information). For the smallest voltages, small notch can be observed together with a protrusion around it, which is characteristic of not having any measurable conduction at all. Above a certain threshold voltage (around 12 V in both cases), the notch diameter is larger and protrusions are smaller, corresponding to conduction after some indentation. Finally, for sufficiently high voltages (typically above 35 V), no protrusions are seen, as illustrated by the cross section.

In the case of exposed SU-8, the results obtained when patterning dots are similar (regardless of the substrate or the applied voltage) and in Figure 4.b a pattern of 12×12 dots made applying a DC voltage of 35V is shown. Protrusions around the indented region can be seen in all the cases.

In addition to dots, the possibility of line patterning was explored and some typical results are shown in the Supporting Information.

3. Discussion

SU-8 formulation contains a Photo Acid Generator (PAG) that, after exposure to UV or electron beam radiation, generates a strong acid, causing the cross-linking of the individual monomers during the post exposure bake (PEB) (see Methods section for further details on SU-8 processing). This turns the exposed resist in a more chemically stable, highly insoluble polymer network. This intrinsic difference between exposed and non-exposed material (please note that the baking temperature is the same for both types of samples) is the cause of all the behavioral differences between them.

The results shown in Figure 1 evidence that for the same material thickness and electrode area, the conduction through the exposed resist is smaller than for the non-exposed case. As mentioned before, when fitting the measured current (above the amplifier noise) to a Fowler-Nordheim tunneling conduction, we can extract (see Supporting Information) a value for the energetic barrier which is double in the case of the exposed resist. The dielectric strength value is around 1750 V/μm in the case of the non-exposed resist and larger than 2250 V/μm in the case of the exposed resist (note that the latter figure is the electric field corresponding to the maximum voltage we are able to apply with our experimental setup, and the actual dielectric strength might be much higher). This means that the insulating properties of the exposed resist (cross-linked material) are far superior to its non-exposed counterpart. The huge values of the dielectric strength (more than one order of magnitude larger than the reported bulk value[33]) are due to the small area tested under our electrodes. If a much larger area was tested (in the order of mm^2), the dielectric strength would most certainly decrease due to point-defects in the resist.

As it has been introduced before, in addition to being more insulating, exposed resist is more stable chemically and less soluble. This is crucial to understand the results from both the indentation experiments and the AFM patterning of the resist layers. We propose three different mechanisms affecting the current: (1) Fowler-Nordheim tunneling, (2) direct contact with the bottom substrate, and (3) oxidation of the substrate. The latter does not apply to gold-coated samples and it is only important for bare silicon substrates (see Supporting Information). The first mechanism depends exponentially of the resist thickness, and thus on the indentation length; but it also depends on the area of conduction, which is affected by the dissolution of resist, in a similar way as reported for PMMA.[23]

When the applied voltages are sufficiently large, conduction starts at the same time than physical contact for non-exposed resist and no protrusion remains after indentation (see Figure 2c). We believe this corresponds to the dielectric breakdown of the resist, which can also be observed in the conduction experiments. As soon as the tip contacts the resist, current flows through it, causing the resist to dissolve and disappear, leaving no trace of protrusion. As it has been stated before, for exposed resist the dielectric breakdown could not be experimentally reached and, therefore, the region where physical and electrical contact start simultaneously is not observed. The resist dissolution is believed to be electrochemical in nature. Experiments performed on SU-8 deposited on bare silicon substrates (see supporting information) show the occurrence of substrate oxidation, indicating ionic transport through the resist, which in turn would generate an electrochemical reaction within the resist. Another possible explanation for the resist removal would be a thermally assisted process, but given the small amount of current flowing through in our experiments, we consider the increase in temperature to be almost negligible.

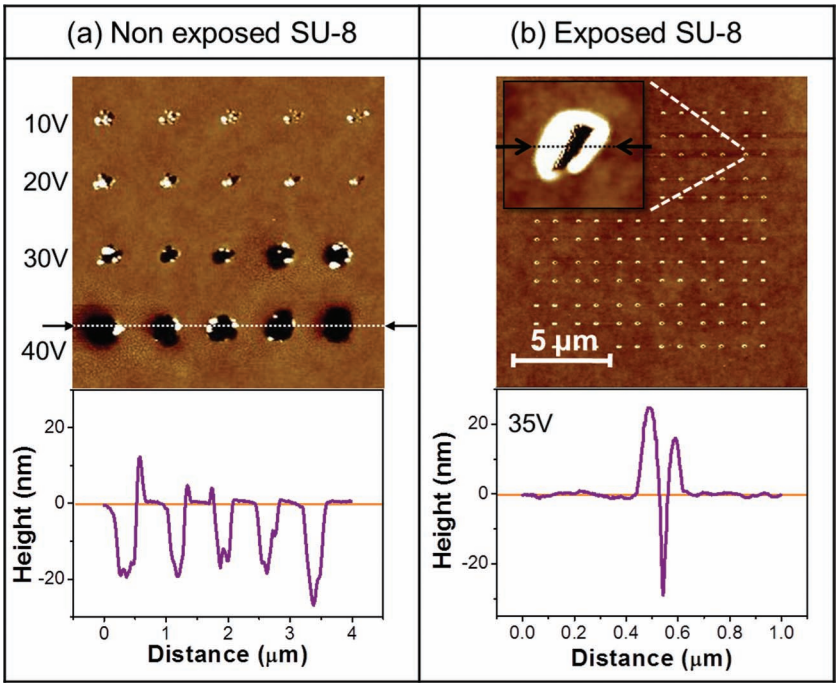

Figure 4. Single nanodots patterning on SU-8 with AFM: Dynamic mode AFM topographic images and respective selected cross-sections (following the dashed lines) taken just after the AFM lithographic processes on 20 nm thick layers of SU-8. a) Non-exposed resist: the threshold for conduction (around 10V) and the point where conduction and contact happen simultaneously (40V) are also apparent. b) Exposed resist: protrusion remains present in all cases, regardless of the applied voltage. We present an array of 12 × 12 holes performed applying 35V between tip and substrate. Inset: zoom in one of the indented holes.

For very small applied voltages, no conduction is observed above the amplifier noise, even after long indentations. This can be understood from the fact that the contact area is originally undefined but very small (of the order of few nm^2). As no appreciable current is flowing, protrusion can be observed as a consequence of polymer displacement during indentation. This can be observed in Figure 2 and 4.

For intermediate voltages, conduction is measurable once the tip is close enough to the substrate. That can happen via tunneling or via direct contact with the substrate through a minute area. In any case, once current is flowing, non-exposed resist starts dissolving, leading to a decrease of the resist thickness around the tip or, alternatively, an increase of the contact area (note that the water meniscus can increase the radius of contact when no resist is present). This is illustrated in Figure 2b, where the current monotonically increases due to the dissolution of the resist, which also causes the reduction (or even disappearance) of the protrusions.

4. Application

The experiments shown before demonstrate that ultrathin SU-8 layers (especially the exposed ones) present highly insulating properties and that their nano-patterning via AFM is feasible. As SU-8 can also be easily patterned via OL, the resist is a very appealing material for the fabrication of nanodevices. We propose here the fabrication of nanoelectrode arrays by using metal and thin-layers of SU-8 as a proof of concept of the possibilities that this resist offers.

Nanoelectrodes are electrodes[34] with a critical dimension (one of the dimensions that control the electrochemical response) smaller than a few hundreds of nanometers. Compared to micro- or macroscopic electrodes, by shrinking their size some benefits are obtained: (1) increase of the Faradaic-to-capacitive current ratio; (2) decrease of the effect of high solution resistance; (3) radial diffusion (diameter much smaller than diffusion length) which causes an increase in mass transport and signal-to-noise ratio; (4) rapid establishment of steady-state limiting currents, which are essentially convection independent.[35,36] In addition, nanoelectrodes are gaining high interest because they can be functionalized and thus show a response caused by only a handful of biomolecules.[37,38] However, due to their ultrasmall sizes, nanoelectrodes provide very small electrical currents (typically in the order of a few pA), which is the main motivation to fabricate nanoelectrode ensembles or arrays (NEAs),[39,40] which can operate as a set of individual electrodes connected in parallel, thus amplifying the signal (when the ratio of the interelectrode distance to the radius of a single electrode is large enough).

AFM modification of polymers for device fabrication has been demonstrated to obtain tunnel nanojunctions.[41] Here, we follow a short and inexpensive fabrication procedure (described in the Supporting Information) to fabricate NEAs of different sizes. Figure 4b shows an AFM image after indenting an array of 12 × 12 nanoelectrodes. The actual size of the aperture is difficult to measure due to tip convolution (logically unavoidable if patterning and imaging are performed with the same tip), but each radius is < 40nm (at the bottom). The space between the apertures is 1 μm.

Figure 5 shows some typical examples of cyclic voltammograms (CV) of a NEA with 10 × 10 electrodes. Figure 5a shows the response for different concentrations of potassium ferrocyanide (1 mM, 5 mM and 10 mM) at a fixed scan rate (50 mVs^{-1}). The sigmoidal shape in the voltammograms is a sign of radial diffusion, as expected from a NEA where the electrode radius is much smaller than the ionic diffusion length. Figure 5b shows a number of sweeps in a 1 mM solution at different scan rates. The observed scan-rate independent limiting current behavior (up to 100 mV s^{-1}) indicates that there is no diffusion layer overlap between the electrodes, which is also expected because the pitch between individual electrodes (apertures on the SU-8) is 1 μm. As the ratio between such pitch and the radius of each aperture (<20 nm) is larger than 40, the conditions for the electrode array to produce sigmoidal shape voltammograms even at fast scan rates are satisfied.[42,43] This enables high speed detection of analytes and investigation of redox processes having fast kinetics.

In addition, as it can be seen in Figure 5b, in our cases the forward and reverse scan curves in the voltammograms are almost identical, indicating very low capacitive current which is

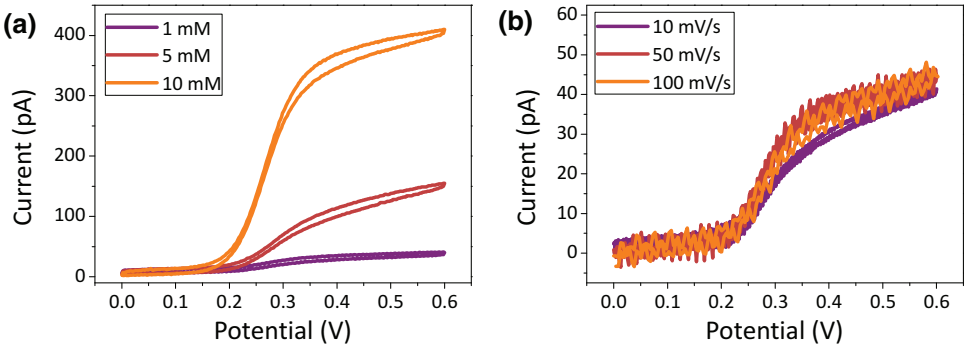

Figure 5. Nanoelectrode behavior: Cyclic voltammograms on a NEA of 10 × 10 apertures in SU-8 in potassium ferrocyanide ($K_4Fe(CN)_6$) with potassium chloride as supporting electrolyte (0.1 M of KCl). a) Typical example of CV in different concentrations of potassium ferrocyanide showing a clear sigmoidal curve, with a scanning speed of 50 mV/s. b) Scan rates of 10, 50 and 100 mV/s showing the scan-rate-independent limiting current behavior and that the capacitive current increments with the increasing scan rate, causing more separation between forward and reverse scans. Potassium ferrocyanide concentration was kept at 1mM.

attributed to the very small electrode sizes. Finally, the current leakage is remarkably small, which is direct consequence of the good insulating properties of exposed SU-8.

5. Conclusions

By performing local electrical measurements of the electrical properties of ultra-thin layers of SU-8, we have found that SU-8 has outstanding insulating properties and enormous dielectric strength (2 orders of magnitude higher than SiO_2). The experiments have also shown that exposed SU-8 is less conductive and more chemically stable than the non-exposed case. We have analyzed and demonstrated the creation of nanopatterns by AFM on ultra-thin film layers of SU-8 and we have elucidated the mechanisms by which the patterns are created: a combination of mechanical indentation and electrochemical dissolution of the resist (for the non-exposed resist) and, in the exposed case, only mechanical indentation (no electrochemical dissolution is observed). Finally, as a proof-of-concept for the applicability of AFM-based lithography on ultrathin SU-8 layers, we have shown the fabrication of NEAs. The prototypes show the expected nanoelectrode behavior, confirming the exceptional insulating properties of the exposed resist and its potential for combination with more established lithography techniques, as OL. The demonstrated technology is flexible, with very low minimum dimensions and relatively high throughput, and therefore can open new avenues for the fabrication of nanodevices.

6. Experimental Section

Sample Preparation: Four different types of samples with SU-8 resist were prepared, as defined by the substrate type (silicon or gold coated silicon) and the condition of the resist (exposed or non-exposed) (See Table S1 in Supporting Information). Silicon samples were obtained by dicing standard 100 mm in diameter p-type <100> Si wafers. For the gold coated samples, wafers of the same type were metalized using a bi-layer of chromium (adhesion layer) and gold (Cr/Au) with respective thicknesses of 2 nm/50 nm. The metals were e-beam evaporated (room temperature, 2×10^{-4} Pa, 2 Å s^{-1}).

Prior to the SU-8 deposition, all the chips were cleaned by dipping them for 1 minute in acetone and 1 minute in isopropyl alcohol (IPA). Then, they were rinsed in deionized water and dried with N_2, and finally dehydrated during 30 minutes at 200 °C in a convection oven, in order to improve adhesion of the resist layer on to the substrates. Spin coating was done at 3000 rpm during 45 seconds with an acceleration of 400 rpm s^{-1}. The resist was then soft baked during 15 minutes in a hot plate, increasing the temperature from 65 °C to 95 °C (with a ramp of 3 °C/min). After this step, all the samples were cleaved, leaving one half with unexposed resist while the other half is locally exposed with ultraviolet radiation (I line). This way, both exposed and unexposed samples have the same thickness, thus allowing the characterization (measuring steps in exposed resist). The exposure dose utilized was 36.4 mJ cm^{-2} and the exposed samples were subsequently baked (post exposure bake, PEB) during 20 minutes in a hot plate, increasing the temperature from 65 °C to 95 °C (with a ramp of 3 °C/min). The resist formulation contains a Photo Acid Generator (PAG) that after the UV-exposure, during the PEB, generates a strong acid which causes the cross-linking of the individual monomers, resulting in an insoluble very dense material. Finally, a developing step was performed (on the exposed samples) in order to remove the non-exposed resist by dipping the samples in Propylene Glycol Methyl Ether Acetate (PGMEA) and rinsed with IPA, deionized water and dried with N_2.

Three different commercially available epoxy based resists have been used for the experiments in this paper: SU-8 2000.5 from Microchem, SU-8 GM1040 from Gersteltech and mr-EBL 6000.1 from Microresist Technology. In order to obtain thin layers (<30 nm) every resist was diluted. We chose to decrease the viscosity of the resists to get our desired thickness when spinning at 3000 rpm. The optimized dilutions are: SU-8 2000.5:cyclopentanone with a ratio 1:20, GM1040:PGMEA with a ratio 1:8, and mr-EBL 6000.1:PGMEA with a ratio 1:2. AFM characterization of the prepared samples showed resist thicknesses between 20-30 nm in all cases and roughness of the resist surface, with or without exposure, lower than 0.5 nm rms.

Sample Preparation for Determination of Insulating Properties of SU-8 Thin Films: In order to make *I–V* curves to find out the volume resistivity for such thin layers, we have deposited Cr/Pt (5/50 nm) electrodes on top of non-exposed and exposed SU-8 thin films by stencil lithography. The stencils were prepared by patterning low stress silicon nitride membranes with holes of approximately 400 nm in diameter.[44] Metallization was performed after fixing the stencil on our substrate and then introducing them into an e-beam evaporator to deposit the bilayer. The deposition was done on substrates with gold deposited underneath the ultra-thin SU-8 layers, both exposed and non-exposed.

AFM Experiments: All the AFM experiments presented in this paper were performed using a Dimension 3100 AFM microscope system with a NanoScope IV controller (from Bruker AXS) in a clean environment

with a temperature of 21.0 ± 0.5 °C and a relative humidity of 50 ± 5%. AFM probes for non-contact (dynamic) mode without coating (nominal values of 40 N/m for the spring constant and 250 kHz for the resonant frequency, supplier Bruker AXS, model RTESP, part MPP-11100-10) have been employed.

In order to measure the current flowing through the AFM tip while applying a voltage between the tip and the substrate, a commercially available current amplifier (I/V converter) was used. This module can detect low-and mid-strength electrical currents, with four different selectable sensitivities (1 pA V^{-1}, 10 pA V^{-1}, 1 nA V^{-1} and 100 nA V^{-1}).

Supporting Information

Supporting Information is available online from the Wiley Online Library or from the author.

Acknowledgements

This work has been financially supported by the EU through 6th framework project "NOVOPOLY" STRP 013619 and the Spanish government through the project TEC2009-14517-C02-01. The authors are very thankful to Anja Voigt and Gabi Gruetzner from Micro Resist Technology for their valuable help.

Received: November 18, 2011
Published online: January 27, 2012

[1] D. Bratton, D. Yang, J. Y. Dai, C. K. Ober, *Polym. Advan. Technol.* **2006**, *17*, 94–103.
[2] H. W. Li, W. T. S. Huck, *Curr. Opin. Solid. St. M.* **2002**, *6*, 3–8.
[3] C. Liu, *Adv. Mater.* **2007**, *19*, 3783–3790.
[4] W. Lee, W. Fon, B. W. Axelrod, M. L. Roukes, *Proc. Natl. Acad. Sci. USA.* **2009**, *106*, 15225–15230.
[5] C. Martin, A. Llobera, G. Villanueva, A. Voigt, G. Gruetzner, J. Brugger, F. Perez-Murano, *Microelectron. Eng.* **2009**, *86*, 1226–1229.
[6] S. Y. Chou, P. R. Krauss, P. J. Renstrom, *Science* **1996**, *272*, 85–87.
[7] A. Genua, J. A. Alduncin, J. A. Pomposo, H. Grande, N. Kehagias, V. Reboud, C. Sotomayor, I. Mondragon, D. Mecerreyes, *Nanotechnology* **2007**, *18*, 215301.
[8] G. Villanueva, O. Vazquez-Mena, M. A. F. van den Boogaart, K. Sidler, K. Pataky, V. Savu, J. Brugger, *Microelectron. Eng.* **2008**, *85*, 1010–1014.
[9] O. Vazquez-Mena, K. Sidler, V. Savu, C. W. Park, L. G. Villanueva, J. Brugger, *IEEE T. Nanotechnol.* **2011**, *10*, 352–357.
[10] A. A. Tseng, *J. Vac. Sci. Technol. B* **2011**, *29*, 040801.
[11] M. Villarroya, F. Perez-Murano, C. Martin, Z. Davis, A. Boisen, J. Esteve, E. Figueras, J. Montserrat, N. Barniol, *Nanotechnology* **2004**, *15*, 771–776.
[12] D. Pires, J. L. Hedrick, A. De Silva, J. Frommer, B. Gotsmann, H. Wolf, M. Despont, U. Duerig, A. W. Knoll, *Science* **2010**, *328*, 732–735.
[13] F. Perez-Murano, G. Abadal, N. Barniol, X. Aymerich, J. Servat, P. Gorostiza, F. Sanz, *J. Appl. Phys.* **1995**, *78*, 6797–6801.
[14] Z. Q. Wei, D. B. Wang, S. Kim, S. Y. Kim, Y. K. Hu, M. K. Yakes, A. R. Laracuente, Z. T. Dai, S. R. Marder, C. Berger, W. P. King, W. A. de Heer, P. E. Sheehan, E. Riedo, *Science* **2010**, *328*, 1373–1376.
[15] R. D. Piner, J. Zhu, F. Xu, S. H. Hong, C. A. Mirkin, *Science* **1999**, *283*, 661–663.
[16] X. Jin, W. N. Unertl, *Appl. Phys. Lett.* **1992**, *61*, 657–659.
[17] H. J. Mamin, D. Rugar, *Appl. Phys. Lett.* **1992**, *61*, 1003–1005.
[18] F. Yang, E. Wornyo, K. Gall, W. P. King, *Nanotechnology* **2007**, *18*, 285302.
[19] H. D. Rowland, W. P. King, J. B. Pethica, G. L. W. Cross, *Science* **2008**, *322*, 720–724.
[20] R. V. Martinez, N. S. Losilla, J. Martinez, M. Tello, R. Garcia, *Nanotechnology* **2007**, *18*, 084021.
[21] M. Lutwyche, C. Andreoli, G. Binnig, J. Brugger, U. Drechsler, W. Haberle, H. Rohrer, H. Rothuizen, P. Vettiger, G. Yaralioglu, C. Quate, *Sens. Actuators, A* **1999**, *73*, 89–94.
[22] P. Vettiger, M. Despont, U. Drechsler, U. Durig, W. Haberle, M. I. Lutwyche, H. E. Rothuizen, R. Stutz, R. Widmer, G. K. Binnig, *IBM J. Res. and Dev.* **2000**, *44*, 323–340.
[23] C. Martin, G. Rius, X. Borrise, F. Perez-Murano, *Nanotechnology* **2005**, *16*, 1016–1022.
[24] S. F. Lyuksyutov, R. A. Vaia, P. B. Paramonov, S. Juhl, L. Waterhouse, R. M. Ralich, G. Sigalov, E. Sancaktar, *Nat. Mater.* **2003**, *2*, 468–472.
[25] S. F. Lyuksyutov, P. B. Paramonov, S. Juhl, R. A. Vaia, *Appl. Phys. Lett.* **2003**, *83*, 4405–4407.
[26] M. R. VanLandingham, S. H. McKnight, G. R. Palmese, J. R. Elings, X. Huang, T. A. Bogetti, R. F. Eduljee, J. W. Gillespie, *J. Adhesion* **1997**, *64*, 31–59.
[27] A. Llobera, G. Villanueva, V. J. Cadarso, S. Buttgenbach, J. A. Plaza, *IEEE Photonic. Tech. L.* **2006**, *18*, 2425–2427.
[28] H. Lorenz, M. Despont, N. Fahrni, J. Brugger, P. Vettiger, P. Renaud, *Sens. Actuators, A* **1998**, *64*, 33–39.
[29] H. Lorenz, M. Laudon, P. Renaud, *Microelectron. Eng.* **1998**, *42*, 371–374.
[30] K. Y. Lee, N. LaBianca, S. A. Rishton, S. Zolgharnain, J. D. Gelorme, J. Shaw, T. H. P. Chang, *J. Vac. Sci. Technol. B* **1995**, *13*, 3012–3016.
[31] C. Martin, G. Rius, A. Llobera, A. Voigt, G. Gruetzner, F. Perez-Murano, *Microelectron. Eng.* **2007**, *84*, 1096–1099.
[32] H. Pozidis, W. Haberle, D. Wiesmann, U. Drechsler, M. Despont, T. R. Albrecht, E. Eleftheriou, *IEEE T. Magnet.* **2004**, *40*, 2531–2536.
[33] J. R. Thorpe, D. P. Steenson, R. E. Miles, *Electron. Lett.* **1998**, *34*, 1237–1238.
[34] *Note that in this section we refer to electrodes in the electrochemical sense of the term.*
[35] J. Hees, R. Hoffmann, A. Kriele, W. Smirnov, H. Obloh, K. Glorer, B. Raynor, R. Driad, N. J. Yang, O. A. Williams, C. E. Nebel, *ACS Nano* **2011**, *5*, 3339–3346.
[36] A. J. Bard, L. R. Faulkner, *Electrochemical methods: Fundamentals and Applications*. **2001**, Weinheim, Germany: Wiley-VCH.
[37] G. Gomila, I. Casuso, A. Errachid, O. Ruiz, E. Pajot, J. Minic, T. Gorojankina, M. A. Persuy, J. Aioun, R. Salesse, J. Bausells, G. Villanueva, G. Rius, Y. Hou, N. Jaffrezic, C. Pennetta, E. Alfinito, V. Akimov, L. Reggiani, G. Ferrari, L. Fumagalli, M. Sampietro, J. Samitier, *Sens. Actuators, B* **2006**, *116*, 66–71.
[38] E. Pajot-Augy, V. Akimov, E. Alfinito, J. Bausells, I. Benilova, I. C. Paramo, A. Errachid, G. Ferrari, L. Fumagalli, G. Gomila, J. Grosclaude, Y. X. Hou, N. Jaffrezic-Renault, C. Martelet, C. Pennetta, M. A. Persuy, M. Pla-Roca, L. Reggiani, S. Rodriguez-Segui, O. Ruiz, R. Salesse, J. Samitier, M. Sampietro, A. P. Soldatkin, J. Vidic, G. Villanueva, *Analog. Integr. Circ. S.* **2008**, *57*, 197–203.
[39] D. W. M. Arrigan, *Analyst* **2004**, *129*, 1157–1165.
[40] J. I. Yeh, H. B. Shi, *Wiley Interdiscip. Rev.-Nanomed. Nanobiotechnol.* **2010**, *2*, 176–188.
[41] K. Bouzehouane, S. Fusil, M. Bibes, J. Carrey, T. Blon, M. Le Du, P. Seneor, V. Cros, L. Vila, *Nano Lett.* **2003**, *3*, 1599–1602.
[42] J. D. Guo, E. Lindner, *Anal. Chem.* **2009**, *81*, 130–138.
[43] H. J. Lee, C. Beriet, R. Ferrigno, H. H. Girault, *J. Electroanal. Chem.* **2001**, *502*, 138–145.
[44] O. Vazquez-Mena, T. Sannomiya, L. G. Villanueva, J. Voros, J. Brugger, *ACS Nano* **2011**, *5*, 844–853.